

# First detection of a deuterated molecule in a starburst environment within NGC 253

J. Butterworth<sup>1</sup>, S. Martín<sup>2,3</sup>, V. M. Rivilla<sup>4</sup>, S. Viti<sup>1,5,6</sup>, R. Aladro<sup>7</sup>, L. Colzi<sup>4</sup>, F. Fontani<sup>8,9,10</sup>, N. Harada<sup>11,12,13</sup>, C. Henkel<sup>14,15</sup>, and I. Jiménez-Serra<sup>4</sup>

<sup>1</sup> Leiden Observatory, Leiden University, PO Box 9513, NL-2300 RA Leiden, the Netherlands  
e-mail: butterworth@strw.leidenuniv.nl

<sup>2</sup> European Southern Observatory, Alonso de Córdova, 3107, Vitacura, Santiago 763-0355, Chile

<sup>3</sup> Joint ALMA Observatory, Alonso de Córdova, 3107, Vitacura, Santiago 763-0355, Chile

<sup>4</sup> Centro de Astrobiología (CAB, CSIC-INTA), Ctra. de Torrejón a Ajalvir km 4, 28850, Torrejón de Ardoz, Madrid, Spain

<sup>5</sup> Transdisciplinary Research Area (TRA) 'Matter'/Argelander-Institut für Astronomie, University of Bonn

<sup>6</sup> Physics and Astronomy, University College London, UK

<sup>7</sup> Elsevier, Radarweg 29, 1043 NX Amsterdam, Netherlands

<sup>8</sup> Istituto Nazionale di Astrofisica (INAF), Osservatorio Astrofisico di Arcetri, Florence, Italy

<sup>9</sup> Max-Planck-Institute for Extraterrestrial Physics (MPE), Garching bei München, Germany

<sup>10</sup> Laboratoire d'Études du Rayonnement et de la Matière en Astrophysique et Atmosphères (LERMA), Observatoire de Paris, Meudon, France

<sup>11</sup> National Astronomical Observatory of Japan, 2-21-1 Osawa, Mitaka, Tokyo 181-8588, Japan

<sup>12</sup> Institute of Astronomy and Astrophysics, Academia Sinica, 11F of AS/NTU Astronomy-Mathematics Building, No.1, Sec. 4, Roosevelt Rd, Taipei 10617, Taiwan

<sup>13</sup> Department of Astronomy, School of Science, The Graduate University for Advanced Studies (SOKENDAI), 2-21-1 Osawa, Mitaka, Tokyo, 181-1855 Japan

<sup>14</sup> Max-Planck-Institut für Radioastronomie, Auf-dem-Hügel 69, 53121 Bonn, Germany

<sup>15</sup> Xinjiang Astronomical Observatory, Chinese Academy of Sciences, 830011 Urumqi, China

Received ; accepted

## ABSTRACT

**Context.** Deuterium was primarily created during the Big Bang Nucleosynthesis (BBN). This fact, alongside its fractionation reactions resulting in enhanced abundances of deuterated molecules, means that these abundances can be used to better understand many processes within the interstellar medium (ISM), as well as its history. Previously, observations of deuterated molecules have been limited to the Galaxy, the Magellanic Clouds and (with respect to HD) to quasar absorption spectra.

**Aims.** We present the first robust detection of a deuterated molecule in a starburst environment and, besides HD, the first one detected outside the Local Group. We therefore can constrain the deuterium fractionation, as observed by DCN.

**Methods.** We observed the CMZ of the nearby starburst galaxy NGC 253 covering multiple Giant Molecular Clouds (GMC) with cloud scale observations ( $\sim 30$  pc) using ALMA. Via the use of the MADCUBA package we were able to perform LTE analysis in order to obtain deuterium fractionation estimates.

**Results.** We detect DCN in the nuclear region of the starburst galaxy NGC 253 and estimate the deuterium fractionation (D/H ratio) of DCN within the GMCs of the CMZ of NGC 253. We find a range of  $5 \times 10^{-4}$  to  $10 \times 10^{-4}$ , relatively similar to the values observed in warm Galactic star-forming regions. We also determine an upper limit of D/H of  $8 \times 10^{-5}$  from DCO<sup>+</sup> within one region, closer to the cosmic value of D/H.

**Conclusions.** Our observations of deuterated molecules within NGC 253 appear to be consistent with previous galactic studies of star forming regions. This implies that warmer gas temperatures increase the abundance of DCN relative to other deuterated species. This study also further expands the regions, particularly in the extragalactic domain, in which deuterated species have been detected.

**Key words.** Interstellar medium (ISM): molecules, galaxies: active - starburst - ISM, astrochemistry.

## 1. Introduction

Deuterium, one of the two stable isotopes of hydrogen, was primarily synthesized during the Big Bang Nucleosynthesis, which occurred during the first seconds after the Big Bang (Epstein et al. 1976; Prodanović & Fields 2003; Cyburt et al. 2016). Deuterium has predominantly been observed in the form of molecules in dense Galactic star-forming cloud cores, and the abundance of these deuterated molecules with respect to their hydrogenated counterparts (D/H  $\sim 10^{-3}$ – $10^{-1}$  Crapsi et al. 2005; Caselli et al. 2008; Colzi et al. 2022) exceeds by orders of mag-

nitude the [D/H] elemental abundance in the Solar neighbourhood ( $\sim 10^{-5}$  Oliveira et al. 2003). Since stars are not a significant source of deuterium, and because deuterium is destroyed in their interior, its abundance, i.e. the D/H ratio, is expected to decrease with cosmic time (Fontani et al. 2011). In fact, observed D-abundance within molecules has been shown to be enhanced due to ongoing chemical processes (Caselli & Ceccarelli 2012).

Deuterium fractionation can result from the formation processes of different deuterated species, which depend on the physical conditions of a region (Colzi et al. 2018, 2022). This frac-

tionation can then result in a column density ratio between a species containing D and its hydrogenated counterpart ( $D_{frac}$ ) higher than the primordial value. As an example, DCN has multiple formation pathways with the primary pathway (62%) being  $\text{HD} + \text{CH}_3^+ \rightarrow \text{CH}_2\text{D}^+$  which then forms CHD and  $\text{CH}_2\text{D}$ , subsequently reacting with N to form DCN (Turner 2001). A secondary formation mechanism (22%) of DCN includes the reaction,  $\text{HD} + \text{H}_3^+ \rightarrow \text{H}_2\text{D}^+$ . However,  $\text{H}_2\text{D}^+$  is also consumed in the sole formation pathway of the deuterated cations  $\text{N}_2\text{D}^+$  and  $\text{DCO}^+$ . These cations are formed most abundantly at low temperatures ( $T < 20\text{K}$ ) where the ratio of  $\text{H}_2\text{D}^+/\text{H}_3^+$  is enhanced (Wootten 1987). Notably, deuterium fractionation ( $D_{frac}$ ) in galactic massive dense cores exhibits values ranging from  $\sim 0.01$  to 0.7, substantially exceeding the primordial D/H ratio (Fontani et al. 2011, 2015; Zahorecz et al. 2017). The [D/H] molecular ratio has been shown to decrease with increasing dust temperature in  $\text{N}_2\text{D}^+$  and its hydrogenated counterpart by Eprecht et al. (2009). Thus, the deuteration fraction becomes a powerful tool to estimate the time since massive stars started heating their medium (Fontani et al. 2014). This fraction may probe the degree of processing of the gas by star formation. DCN on the other hand is primarily enhanced in warmer gas (up to  $\sim 70\text{K}$ . Roueff et al. 2013; Fontani et al. 2015; Gerner et al. 2015). Thus, processes that influence the temperature of an environment, such as shocks may also affect the deuterium fractionation. This is seen in the deuterium fractionation of DCN/HCN within shocked galactic regions like L1157-B1, which are associated with particularly high DCN/HCN abundance ratios (Busquet et al. 2017).

Lyman Limit System (LLS) measurements, in the line of sight high- $z$  quasars ( $z \sim 2.5$ ) indicate a primordial D/H ratio of around  $2.55 \pm (0.03) \times 10^{-5}$  (Zavarygin et al. 2018). In the Galactic Center (GC), where matter has undergone particularly intense stellar processing, even lower D/H ratios are expected. The GC also typically possesses high kinetic temperatures ( $T_{kin}$ ), thus deuteration is not expected to be efficient. There are 2 studies that have derived the D/H ratio within the Galactic center. Firstly, a study by Lubowich et al. (2000) identified a deuterium to hydrogen of ( $D/H \sim 1.7 \times 10^{-6}$ ) within the Galactic bulge; this value was five orders of magnitude above the value of  $5 \times 10^{-12}$  within the central bulge of the Milky Way, as predicted by nucleosynthesis models within this region. Such enhancement was claimed to result from pristine material feeding the central molecular zone of our Galaxy. Surprisingly, however, measurements in GC star-forming regions report [D/H] values of  $2 - 4 \times 10^{-4}$ , derived from deuterated molecular species (Colzi et al. 2022). In this work the authors used the high D/H ratio to pinpoint positions in the GC where a future generation of stars will form.

Despite extensive studies in the Milky Way, extragalactic investigations of deuterium fractionation remain limited due to observational challenges. Notable exceptions include detections of deuterated molecular hydrogen (HD) in absorption towards damped Lyman- $\alpha$  systems (Ivanchik et al. 2010). There are also reported detections of deuterated species (such as  $\text{DCO}^+$ ) towards star-forming regions in the Large Magellanic Cloud (LMC) with an estimated D/H ratio of  $\sim 10^{-4}$  (Chin et al. 1996; Heikkilä et al. 1997). However, the information towards even the nearest and brightest galaxies consists of upper limits or tentative detections of DCN towards a couple of sources (Mauersberger et al. 1995). In particular, DCN and  $\text{N}_2\text{D}^+$  have been tentatively observed towards the starbursting environment of NGC 253 by Martín et al. (2006). Martín et al. (2006) obtained an upper limit for DCN,  $\text{DCO}^+$  and a tentative detection of  $\text{N}_2\text{D}^+$  resulting in

a D/H ratio of  $< 1 - 4 \times 10^{-3}$  for these molecules at low spatial resolution ( $\sim 300\text{pc}$ ).

In this paper, we present the first robust detection of a deuterated molecule in a non-Magellanic Cloud extragalactic starburst environment, the starburst galaxy NGC 253, which is (besides HD) also the first detection of such a molecule outside the Local Group. We hence derive for the first time a robust D/H ratio and compare it with both galactic ratios and those observed within the LMC, as well as with theoretical models. By examining deuterated species, we seek to uncover clues about the evolutionary state of star-forming regions and the impact of galaxy-scale processes on deuterium enrichment.

## 2. Observations

We carried out interferometric observations using the Atacama Large Millimeter/Submillimeter Array (ALMA) in Cycle 5 in the period between June and August 2018 as part of the project 2017.1.00028.S. The observations were centered at the coordinates  $\alpha_{J2000.0} = 0^h 47^m 33.182^s$  and  $\delta_{J2000.0} = -25^\circ 17' 17.148''$ . We used two different spectral setups: one in Band 4 to target the  $J=2-1$  transitions of the deuterated species DCN,  $\text{DCO}^+$ , and  $\text{N}_2\text{D}^+$ , and one in Band 5 to target the same transition of the hydrogenated species  $\text{H}^{13}\text{CN}$ ,  $\text{H}^{13}\text{CO}^+$ , and  $\text{N}_2\text{H}^+$  (see Table 1). The information of the observations in each band (date, number of antennas, range of baselines, time on source, rms, system temperatures and precipitable water vapour) are summarized in Table 2.

The data was calibrated and imaged using standard ALMA calibration scripts of the Common Astronomy Software Applications package (CASA) (CASA Team et al. 2022)<sup>1</sup>. We used the CASA task *tclean*, with the *auto-multithresh* option, which automatically masks regions during the cleaning process. We chose a common beam for all the spectral datacubes on Band 4 and 5 of  $1.6'' \times 1.2''$  and  $\text{PA} = 80^\circ$ . The continuum was subtracted in the image plane using the STATCONT<sup>2</sup> package (Sánchez-Monge et al. 2017). The expected flux density calibration uncertainty is of 5%, as estimated from recent analysis of calibrators in bands 3 and 6 (Bonato et al. 2018; Remijan et al. 2019, and references therein). The integrated spectral line intensities from our data cubes were extracted using CubeLineMoment<sup>3</sup> (Mangum et al. 2019). CubeLineMoment works by extracting integrated intensities for a given list of targeted spectral frequencies by applying a set of spectral and spatial masks (defined by the user). The CubeLineMoment masking process uses a brighter spectral line (typically the main isotopologue line of the same rotational transition), whose velocity structure over the galaxy is most representative of the science target line, which is used as a tracer of the velocity of the inspected gas component. The products of CubeLineMoment are moment 0, 1, and 2 maps in the units chosen by the user, masked below a chosen  $\sigma$  threshold (channel-based).

## 3. Analysis and results

In this paper we present the first observed spectra of a deuterated species detected within an extra-galactic starburst environment. Using observations of deuterated DCN in combination with the

<sup>1</sup> <https://casa.nrao.edu>

<sup>2</sup> STATCONT is a python-based tool designed to determine the continuum emission level in line-rich spectral data; <https://hera.ph1.uni-koeln.de/sanchez/statcont>

<sup>3</sup> <https://github.com/keflavich/cube-line-extractor>

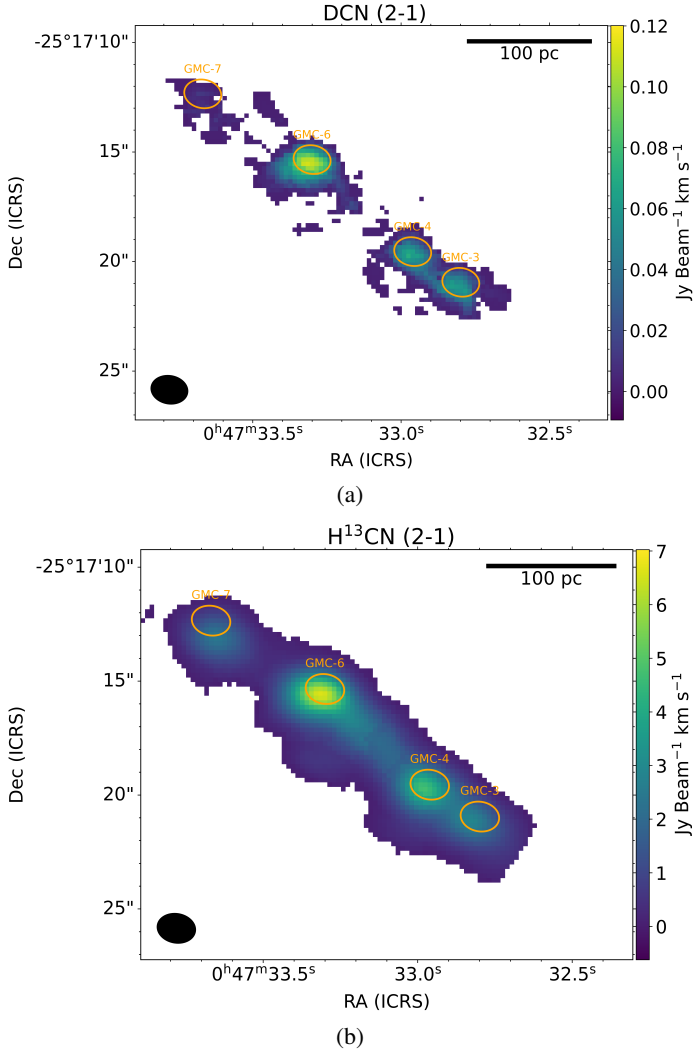


Fig. 1: Velocity-integrated line intensity moment 0 maps, given in  $[\text{Jy km s}^{-1}/\text{beam}]$ , for the observed DCN (2-1) line (a) alongside the accompanying  $\text{H}^{13}\text{CN}$  (2-1) line (b). Both of these maps are shown with a 3 sigma cut off. The orange ellipses show the beam-sized regions over which the later analysis of this letter was conducted.

Table 1: Spectroscopy of the deuterated molecular transitions and of their hydrogenated counterparts studied in this work from CDMS (Müller et al. 2001, 2005; Endres et al. 2016). The spectroscopic information of additional lines used in this paper are given in Appendix A.

Molecule	Frequency (GHz)	Transition	$\log A_{ul}$ ( $\text{s}^{-1}$ )	$E_{up}$ (K)
DCN	144.8280015	2-1	-3.89786	10.4
$\text{H}^{13}\text{CN}$	172.6778512	2-1	-3.67033	12.4
$\text{DCO}^+$	144.0772890	2-1	-3.18099	10.4
$\text{H}^{13}\text{CO}^+$	173.5067003	2-1	-3.43195	12.5
$\text{N}_2\text{D}^+$	154.2170318	2-1	-3.70470	11.1
$\text{N}_2\text{H}^+$	186.3446844	2-1	-3.45807	13.4

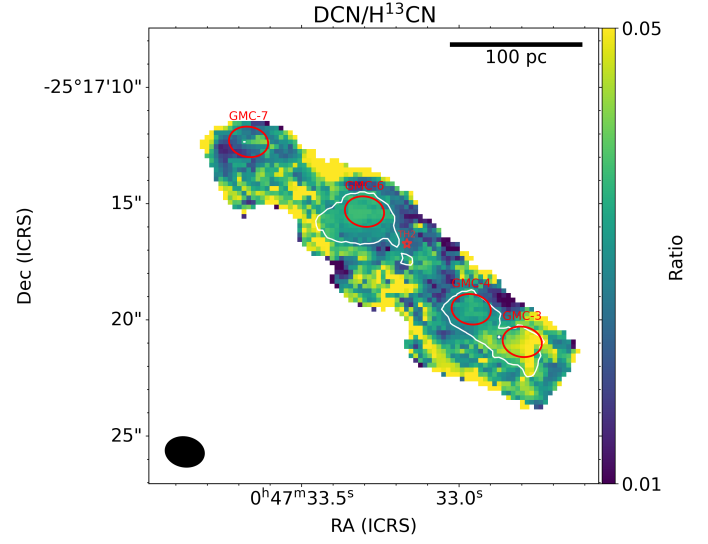


Fig. 2: The ratio map of the velocity integrated line intensities of DCN (2-1)/ $\text{H}^{13}\text{CN}$  (2-1). The white contours shown are the 5 sigma limited intensities of DCN (2-1).

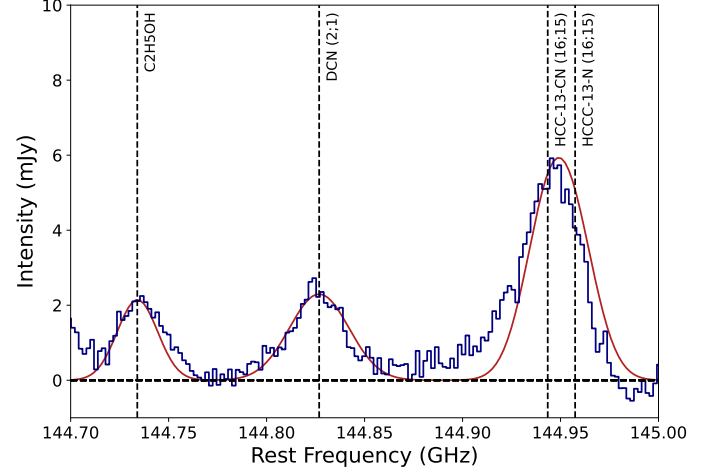


Fig. 3: DCN (2-1) spectrum observed in the brightest region GMC-6 (in blue). The best fitting LTE model from MADCUBA is shown overplotted in red.

hydrogenated isotopologue  $\text{H}^{13}\text{CN}$  we have computed an estimate of the D/H ratio towards four GMC regions within the NGC 253 central molecular zone. These GMC regions are based upon both continuum and molecular line emission observations previously defined within NGC 253 (e.g. Leroy et al. 2015, 2018; Levy et al. 2022). Specifically, the four innermost GMCs are studied, GMC-4, 5, 6 and 7. The detections of DCN within these regions are provided alongside upper limits of the deuterium fractionation from the deuterated species  $\text{DCO}^+$  and  $\text{N}_2\text{D}^+$ . The integrated intensities of each line within each region are shown in Table 3. In Figure 1 we present the velocity-integrated line intensity moment 0 maps from DCN (2-1) and  $\text{H}^{13}\text{CN}$  (2-1) obtained via CubeLineMoment. The moment 0 maps of both  $\text{N}_2\text{H}^+$  (2-1) and  $\text{H}^{13}\text{CO}^+$ , alongside the moment 0 maps of the two  $\text{HC}_3\text{N}$  lines used as a part of this study are shown in Appendix B. The ratio map of DCN/ $\text{H}^{13}\text{CN}$  is given in Figure 2.

To conduct our analysis we have used the SLIM (Spectral Line Identification and Modeling) tool within the MAD-

Table 2: The parameters of the ALMA observations used as a part of this study.

Band	Date	#	Baselines	$t_{\text{OS}}^{(a)}$	$rms^{(b)}$	$T_{\text{sys}}$	$pwv^{(c)}$
	2018	Antennas	(m)		(mJy/beam)	(K)	(mm)
4	June & Aug.	46–48	15–782	4.5 h	0.38	52–90	0.4–4.6
5	Aug.	46	15–500	15 min	0.56	140	0.5

(a) Time on the source NGC 253. (b) Measured in  $10 \text{ km s}^{-1}$ . (c) Precipitable water vapour.

CUBA package (Martín et al. 2019)<sup>4</sup> which allows us to identify and perform multi-transition profile fitting. To accomplish this, SLIM generates a synthetic spectrum, assuming local thermodynamic equilibrium (LTE) conditions, and finds the best nonlinear least-squares fit to the data as well as the associated statistical errors. The free parameters to be fitted are the column density of the molecule,  $N_{\text{mol}}$ , the excitation temperature,  $T_{\text{ex}}$ , the peak velocity,  $v_{\text{LSR}}$ , and the full width at half maximum (FWHM). In this paper, due to being limited to a single line in both DCN and  $\text{H}^{13}\text{CN}$ , the parameter that was left free was the column density  $N_{\text{mol}}$ . In order to derive the temperature within each region we decided to use the serendipitous detection of multiple lines of  $\text{CH}_3\text{CCH}$ .  $\text{CH}_3\text{CCH}$  is a molecule with a known population dependence on kinetic temperature. As a result of it being a symmetric top molecule  $\text{CH}_3\text{CCH}$  possesses a dipole moment in line with its carbon chain. This means that transitions with  $\Delta k > 0$  are forbidden (where  $k$  is the projection of the total angular momentum,  $J$ , on the rotational axis). Thus, different  $K$ -components are connected only via collisional processes, making their relative population sensitive to the kinetic temperature (Fayolle et al. 2015; Calcutt et al. 2019; Ben Khalifa et al. 2024). Due to the complex hyperfine structure of  $\text{CH}_3\text{CCH}$  we were able to observe multiple lines of the  $J = 9-8$  and  $J = 11-10$  transitions. The temperatures for each region are given in Table 4. The resulting  $T_{\text{ex}}$  from  $\text{CH}_3\text{CCH}$  has been shown to be a good estimate of the kinetic temperature of the gas at densities of  $n_{\text{H}} \geq 10^{3-4} \text{ cm}^{-3}$  (Askne et al. 1984; Bergin et al. 1994). The source size of each region was assumed to be equal to the beam size, and thus the beam-sized region intensities were extracted. To perform the LTE line fitting we use the MADCUBA AUTOFIT function which provides the best solution for the free parameters, and their associated errors. Also,  $\text{H}^{13}\text{CN}$  has been found to be optically thin within NGC 253, and thus likely DCN too, at similar regions at the similar spatial scales (Butterworth et al. 2024). This was tested in MADCUBA, varying the the  $T_{\text{ex}}$  within the LTE modelling had a negligible effect

To determine the D/H ratios in each region the column density of  $\text{H}^{13}\text{CN}$  has been converted to the column density of the primary isotopologue (HCN) by determining the  $^{12}\text{C}/^{13}\text{C}$  ratio from the simultaneously observed  $\text{HC}_3\text{N}$  and two of its prominent isotopologues,  $\text{HC}^{13}\text{CCN}$  and  $\text{HCC}^{13}\text{CN}$ . The calculated  $^{12}\text{C}/^{13}\text{C}$  ratios ranged from  $\sim 40-56$  across the 4 regions. These values are on the high end but are relatively consistent with the ratio derived by Martín et al. (2021) using  $\text{HC}_3\text{N}$  at  $16''$  resolution towards NGC 253; they are also consistent with the  $^{12}\text{C}/^{13}\text{C}$  ratio obtained by Tang et al. (2019) using ALMA observations of CN and its  $^{13}\text{C}$ -bearing isotopologue within NGC 253. Table 4 lists the obtained D/H ratios for each GMC region as indi-

cated by DCN as well as the estimated upper limits for  $\text{N}_2\text{D}^+$  and  $\text{DCO}^+$ . DCN (2-1) benefits from not having many nearby lines potentially contaminating the detection. Thanks to the broadband spectral scan carried out by ALMA (ALCHEMI, Martín et al. 2021) we can safely confirm the lack of contamination by known species. Of known lines at the same frequency as DCN (2-1) at the redshift of NGC 253, they are only of either complex species not previously observed in extragalactic sources, or low intensity hyperfine structure lines from species such as  $\text{CH}_3\text{OH}$  (Endres et al. 2016). For each of these cases of unknown lines we can say with some assurance that they are not contaminating the DCN (2-1) detection within our regions. While the low resolution data published by Martín et al. (2021) does not indicate the presence of DCN, the full spectral modelling of the high resolution data (Lopez-Gallifa in prep.) shows hints of the emission of DCN in four different transitions from 144 GHz to 362 GHz. The transition reported here is the only one not blended with emission from other species as shown in Fig. 3. We note that the data presented here are much deeper than those reached in the ALCHEMI data. The spectra of all four GMC regions for all investigated lines are given in Appendix C.

#### 4. Discussion and Conclusions

Observing deuterated species in extragalactic environments is key to understanding deuteration processes within the ISM of galaxies. The degrees of fractionation observed in DCN/HCN in NGC 253 are consistent with similar galactic CMZ studies covering regions of similar kinetic temperatures (e.g. Colzi et al. 2022).

In order to properly interpret our results we shall compare our observed values and upper limits of D/H to those observed in other sources. In Figure 4, we show how the D/H ratio from column density ratios and the line intensity ratios of DCN (2-1)/ $\text{H}^{13}\text{CN}$  (2-1) compare to the recent galactic D/H ratio obtained from DCN by Colzi et al. (2022). The intensity and column density ratios as shown in Figure 4 generally agree in each of the GMCs. Colzi et al. (2022) observed two components within G+0.693-0.027, a molecular cloud located within the Sgr B2 complex of the Milky Way's central molecular zone. Using Non-LTE Radiative Transfer modelling they were able to identify physical conditions of a prestellar (PS) component ( $T_K \sim 30\text{K}$ ) and a broad warm component ( $T_K \sim 100\text{K}$ ). These components were observed with varying deuterium fractionations as observed with isotopologues of dense gas tracers, such as HCN,  $\text{HCO}^+$  and HNC. When comparing to the results of Colzi et al. (2022) it can be seen that GMC-6 is quite comparable to the broad, warmer component of G+0.693-0.027. The D/H ratio of  $(10.3 \pm 0.1) \times 10^{-4}$  we observe towards GMC-6 is comparable to the  $(8.6 - 13) \times 10^{-4}$  observed in G+0.693-0.027's broad component by Colzi et al. (2022) also using DCN. The broad component of G+0.693-0.027 and the gas component

<sup>4</sup> Madrid Data Cube Analysis on ImageJ which is a software developed in the Center of Astrobiology (CAB, CSIC-INTA) to visualize and analyze astronomical single spectra and datacubes. MADCUBA is available at <https://cab.inta-csic.es/madcuba/>

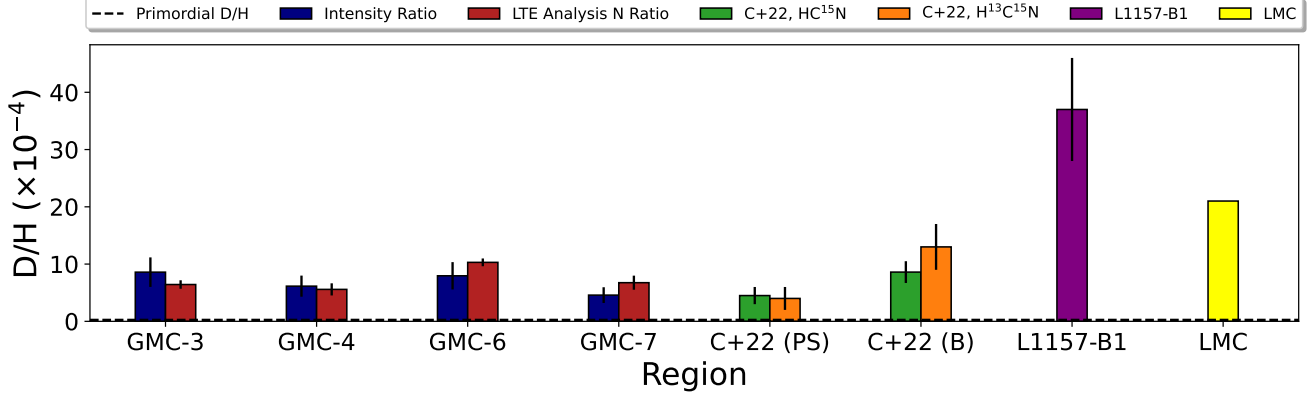


Fig. 4: The D/H as obtained through DCN for each region across NGC 253, shown both for the intensity ratio of DCN (2-1)/H<sup>13</sup>CN (2-1) (in blue) and column density ratio (in red). These observations are shown relative to the prestellar (PS) and broad (B) components of G+0.693-0.027 from Colzi et al. (2022) (C+22, shown in green and orange, respectively), the D/H ratio observed in the shock region L1157-B1 by Busquet et al. (2017) (in purple) and the DCN/HCN ratio observed in the LMC by Chin et al. (1996) (in yellow).

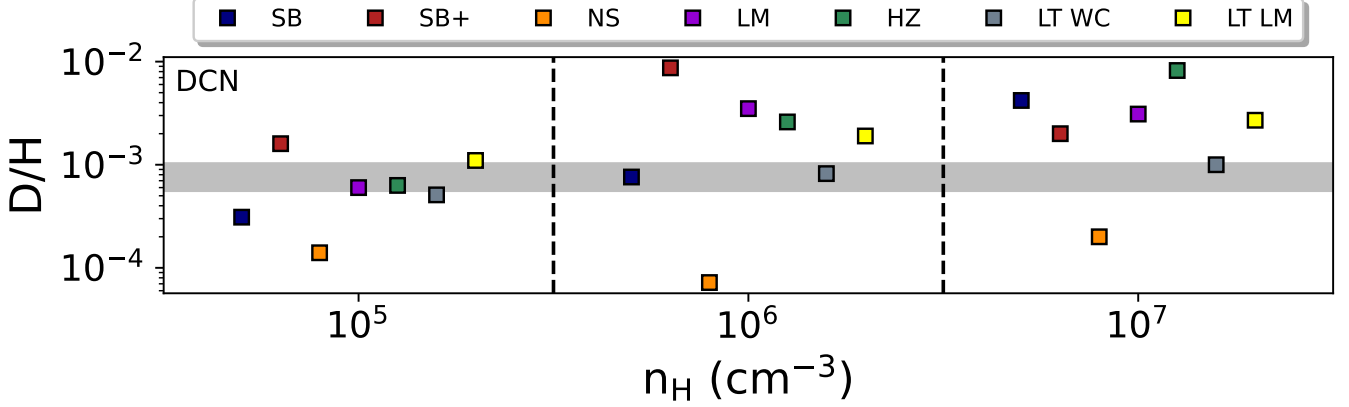


Fig. 5: Comparison of LTE analysis Predicted Column density ranges of DCN/HCN to models shown in Roueff et al. (2007) and Bayet et al. (2010). SB stands for Starburst, SB+ for Cosmic-ray enhanced starburst, NS for Normal Spiral, LM for Low Metallicity, HZ for High redshift and WC for Warm Core. The LT (Lower Temperature) prefix is given to the models from Roueff et al. (2007) as these models were conducted at a significantly lower kinetic temperature (70 K), than the remaining models from Bayet et al. (2010) (>300 K). The effect of this temperature difference is discussed in the text. The primordial D/H ratio of around  $2.55 \pm (0.03) \times 10^{-5}$  is presented with a horizontal dashed line (Zavarygin et al. 2018).

Table 3: Integrated intensities in [K km s<sup>-1</sup>] as observed within each of the studied GMC regions. The errors presented represent 1 $\sigma$ . The integrated intensities are provided only for the non-contaminated lines.

Molecule	Transition	Intensities (K km s <sup>-1</sup> )			
		GMC-3	GMC-4	GMC-6	GMC-7
H <sup>13</sup> CN	(2-1)	42.7±6.4	72.4±10.9	95.7±14.4	35.0±5.2
DCN	(2-1)	1.9±0.3	2.3±0.3	3.4±0.5	1.0±0.1
N <sub>2</sub> H <sup>+</sup>	(2-1)	82.7±12.4	191.0±28.6	173.0±25.9	99.1±14.9
H <sup>13</sup> CO <sup>+</sup>	(2-1)	47.8±7.2	67.6±10.1	88.6±13.3	16.6±2.5

Table 4: The deuterium fractionations for each GMC region shown for DCN as well as the 1 sigma upper limits obtained for DCO<sup>+</sup> and N<sub>2</sub>D<sup>+</sup> as a result of the LTE fitting conducted using MADCUBA, the T<sub>ex</sub> for each region are also provided.

Region	DCN/HCN ( $\times 10^{-4}$ )	DCO <sup>+</sup> /HCO <sup>+</sup> ( $\times 10^{-4}$ )	N <sub>2</sub> D <sup>+</sup> /N <sub>2</sub> H <sup>+</sup> ( $\times 10^{-3}$ )	T <sub>ex</sub> (K)	FWHM (km s <sup>-1</sup> )	<sup>12</sup> C/ <sup>13</sup> C
GMC-3	6.43 ± 0.74	(< 1.51)	(< 4.47)	50 ± 5	74	48 ± 4
GMC-4	5.58 ± 1.06	(< 0.8)	(< 2.51)	60 ± 7	74	57 ± 10
GMC-6	10.3 ± 0.1	(< 1.08)	(< 3.02)	98 ± 4	74	41 ± 2
GMC-7	6.75 ± 1.23	(< 5.49)	(< 4.17)	61 ± 11	79	44 ± 5

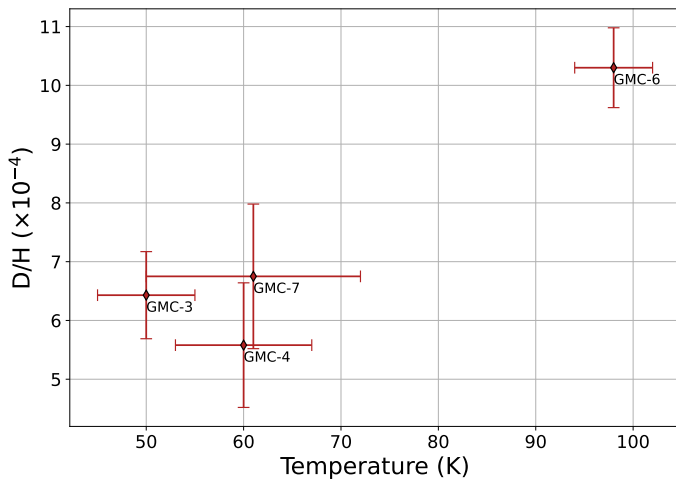


Fig. 6: Derived excitation temperatures of DCN from LTE analysis versus the predicted deuterium fractionation derived for DCN across the GMC regions.

traced by DCN and H<sup>13</sup>CN, within GMC-6, in this project both also seem to have comparable kinetic temperatures ( $\sim 100$  K). GMCs -4,-5 and -7 on the other hand each have DCN/HCN fractions ( $D/H = 5.58 - 6.75 \times 10^{-4}$  which lie between that observed by the cooler prestellar component,  $D/H \sim 4 \times 10^{-4}$ ) and the broad component of G+0.693-0.027,  $D/H = (8.6 - 13) \times 10^{-4}$ . This is consistent with the observed temperatures of these regions ( $\sim 60$  K, shown in Table 4 which are predicted to both being warmer than the cooler prestellar region of G+0.693-0.027 but less warm than the broad warm component. This all implies a similarity between the CMZ of NGC 253 and our own galaxy. The upper limit D/H ratio as derived from a tentative detection of DCO<sup>+</sup> is  $< 8 \times 10^{-5}$ , within GMC-4, which is relatively similar to the cosmic value of  $\sim 2 \times 10^{-5}$  (Zavarygin et al. 2018). It is also important to note that Colzi et al. (2022) detected similarly low D/H ratios within the broad component of G+0.693-0.027 through N<sub>2</sub>D<sup>+</sup> and DCO<sup>+</sup> and their hydrogenated counterparts.

When comparing our deuterium fractions to those observed within the LMC using DCN by Chin et al. (1996) we see that they appear to be low relative to their  $\sim 2 \times 10^{-3}$ . It should be noted that the LMC is a known low metallicity environment and thus this may contribute to the relatively high deuterium fraction observed, since the LMC gas is less contaminated by stellar processing, negatively affecting the deuterium abundance.

Finally, we compare our D/H values to those observed in a shocked region. The shocked molecular outflow region L1157-B1 was observed by Busquet et al. (2017) to have D/H values of the order higher than observed within this study at  $D/H \sim 4 \times 10^{-3}$ . The predicted temperatures of this region of 80 K are also relatively consistent with those predicted for the regions of this study. As can be seen in Figure 4 the observed D/H fraction within this region is significantly higher, implying an enhancement on the deuterium fractionation by shocks.

It is also important to compare our observed D/H ratios to those predicted by appropriate chemical modelling. Figure 5 shows how the range of D/H ratios across the GMC regions compares to previous investigations of this ratio in DCN/HCN using chemical models from Roueff et al. (2007) and Bayet et al. (2010). In theory the most appropriate model for the conditions of GMCs within the CMZ of NGC 253 would be that of the cosmic-ray enhanced starburst environments (denoted as ‘SB+’) from Bayet et al. (2010), specifically the  $10^6$  cm<sup>-3</sup> density case (similar to the density derived by Mangum et al. 2019). The ‘SB+’ is in full agreement with the enhanced cosmic ray ionization rate towards the central molecular zone of NGC 253 probed by various molecular species (Holdship et al. 2021; Harada et al. 2021; Holdship et al. 2022; Behrens et al. 2022). As can be seen in Figure 5 however, this model significantly over predicts the DCN/HCN ratio relative to what we have observed. The D/H

ratio appears to increase in GMC-6 relative to the other 3 regions and this also corresponds to a significantly higher temperature in GMC-6 relative to the other GMCs; a plot showing this trend can be seen in Figure 6. The ‘SB+’ model in Bayet et al. (2010) was run with a temperature of 300 K which is significantly higher than the temperature range we probe with these observations (~50-100K). DCN is favoured to form from HD present in warmer gas and so this may explain the overprediction in the Bayet et al. (2010) models. The models from Roueff et al. (2007) were run using more comparable temperatures (50-70 K) and as can be seen in Figure 5 the warm core model at a density of  $10^6 \text{cm}^{-3}$  and temperature of 70 K fits very well with our observations, as they also do to the broad component of G+0.693-0.027 studied by Colzi et al. (2022). This may also suggest that the cosmic ray ionisation rate is not important for deuterium fractionation processes.

Approaching the warmer temperatures of the gas traced by these molecules (> 60 K) the most efficient formation mechanism for DCN in the ISM is that of  $\text{CH}_2\text{D}^+$  reacting with atomic N (Roueff et al. 2007, 2013). The  $\text{CH}_2\text{D}^+$  is formed by the exothermic reaction



which becomes the primary processing reaction of HD (the most abundant deuterated species) at >50 K. The  $\text{CH}_2\text{D}^+$  then reacts with the atomic N, in the following reaction



The  $\text{DCN}^+$  cation then undergoes hydrogenation and dissociative recombination reactions to form DCN. Roueff et al. (2007) performed chemical models at 50-70 K and observed D/H ratios in DCN and HCN of  $> 5 \times 10^{-4}$ , which are consistent with the observed results of this paper.

In conclusion the results of this paper are:

- Observing DCN within the CMZ of NGC253 is advantageous thanks to the relatively close proximity of this galaxy. Our observation provides us with the opportunity to study deuteration in star-forming regions at cloud-scale resolution despite the limited spatial resolution inherent to extragalactic studies. As described in Section 1, NGC 253 contains multiple well observed GMCs as well as in Super Star Clusters (SSCs).
- We were able to constrain D/H ratio estimates within 4 regions of the CMZ of NGC 253 via isotopologues of HCN. We obtained a range between  $5.58 \pm 1.06 \times 10^{-4}$  and  $10.3 \pm 0.1 \times 10^{-4}$  across the 4 GMCs. The warmest observed region, GMC-6, comparing favourably to the warm, broad component of G+0.693-0.027 observed within the CMZ of our Galaxy. The remaining 3 GMCs, each with cooler predicted temperatures aligned more closely to the cooler prestellar component observed within G+0.693-0.027 as observed by Colzi et al. (2022).
- Our results seem to be consistent with the idea that warmer temperature gas components lead to an increase in the abundance of DCN.
- In order to be more certain of the exact conditions of the gas being traced by DCN, other species such as  $\text{N}_2\text{D}^+$  and  $\text{DCO}^+$  need to be detected, as thanks to their preference of lower temperature formation mechanisms the correlation between deuterium fractionation and temperature could be better constrained in these extragalactic studies.

To conclude, in this paper we have shown the first detection of a deuterated molecule in an extragalactic starburst environment, beside the LMC. This study provides another step in the progression of the study of deuterated species in the ISM by providing a comparison to the numerous observations of deuterated molecules within our own Galaxy.

## Acknowledgements

This paper makes use of the following ALMA data: ADS/JAO.ALMA#2017.1.00028.S ALMA is a partnership of ESO (representing its member states), NSF (USA) and NINS (Japan), together with NRC (Canada), NSTC and ASIAA (Taiwan), and KASI (Republic of Korea), in co-operation with the Republic of Chile. The Joint ALMA Observatory is operated by ESO, AUI/NRAO and NAOJ. J.B. and S.V. have received funding from the European Research Council (ERC) under the European Union’s Horizon 2020 research and innovation programme MOPPEX 833460. V.M.R. and LC acknowledge support from the grants No. PID2019-105552RB-C41 and PID2022-136814NB-I00 by the Spanish Ministry of Science, Innovation and Universities/State Agency of Research MICIU/AEI/10.13039/501100011033 and by "ERDF A way of making Europe". VMR also acknowledges support from the grant RYC2020-029387-I funded by MICIU/AEI/10.13039/501100011033 and by "ESF, Investing in your future", from the Consejo Superior de Investigaciones Científicas (CSIC) and the Centro de Astrobiología (CAB) through the project 20225AT015 (Proyectos intramurales especiales del CSIC); and from the grant CNS2023-144464 funded by MICIU/AEI/10.13039/501100011033 and by “European Union NextGenerationEU/PRTR”. The authors would like to thank the anonymous referee for the constructive comments that greatly increased the quality of this paper from its original version.

## References

- Askne, J., Hoglund, B., Hjalmarsen, A., & Irvine, W. M. 1984, *A&A*, 130, 311  
 Bayet, E., Awad, Z., & Viti, S. 2010, *ApJ*, 725, 214  
 Behrens, E., Mangum, J. G., Holdship, J., et al. 2022, *ApJ*, 939, 119  
 Ben Khalifa, M., Darna, B., & Loreau, J. 2024, *A&A*, 683, A53  
 Bergin, E. A., Goldsmith, P. F., Snell, R. L., & Ungerechts, H. 1994, *ApJ*, 431, 674  
 Bonato, M., Liuzzo, E., Giannetti, A., et al. 2018, *MNRAS*, 478, 1512  
 Busquet, G., Fontani, F., Viti, S., et al. 2017, *A&A*, 604, A20  
 Butterworth, J., Viti, S., Van der Werf, P. P., et al. 2024, *A&A*, 686, A31  
 Calcutt, H., Willis, E. R., Jørgensen, J. K., et al. 2019, *A&A*, 631, A137  
 CASA Team, Bean, B., Bhatnagar, S., et al. 2022, *PASP*, 134, 114501  
 Caselli, P. & Ceccarelli, C. 2012, *A&A Rev.*, 20, 56  
 Caselli, P., Vastel, C., Ceccarelli, C., et al. 2008, *A&A*, 492, 703  
 Chin, Y. N., Henkel, C., Millar, T. J., Whiteoak, J. B., & Mauersberger, R. 1996, *A&A*, 312, L33  
 Colzi, L., Fontani, F., Rivilla, V. M., et al. 2018, *MNRAS*, 478, 3693  
 Colzi, L., Romano, D., Fontani, F., et al. 2022, *A&A*, 667, A151  
 Crapsi, A., Caselli, P., Walmsley, C. M., et al. 2005, *ApJ*, 619, 379  
 Cyburt, R. H., Fields, B. D., Olive, K. A., & Yeh, T.-H. 2016, *Reviews of Modern Physics*, 88, 015004  
 Emprechtinger, M., Caselli, P., Volgenau, N. H., Stutzki, J., & Wiedner, M. C. 2009, *A&A*, 493, 89  
 Endres, C. P., Schlemmer, S., Schilke, P., Stutzki, J., & Müller, H. S. P. 2016, *Journal of Molecular Spectroscopy*, 327, 95  
 Epstein, R. I., Lattimer, J. M., & Schramm, D. N. 1976, *Nature*, 263, 198  
 Fayolle, E. C., Öberg, K. I., Garrod, R. T., van Dishoeck, E. F., & Bisschop, S. E. 2015, *A&A*, 576, A45  
 Fontani, F., Busquet, G., Palau, A., et al. 2015, *A&A*, 575, A87  
 Fontani, F., Palau, A., Caselli, P., et al. 2011, *A&A*, 529, L7  
 Fontani, F., Sakai, T., Furuya, K., et al. 2014, *MNRAS*, 440, 448  
 Gerner, T., Shirley, Y. L., Beuther, H., et al. 2015, *A&A*, 579, A80  
 Harada, N., Martín, S., Mangum, J. G., et al. 2021, *ApJ*, 923, 24

- Heikkilä, A., Johansson, L. E. B., & Olofsson, H. 1997, A&A, 319, L21
- Holdship, J., Mangum, J. G., Viti, S., et al. 2022, ApJ, 931, 89
- Holdship, J., Viti, S., Martín, S., et al. 2021, A&A, 654, A55
- Ivanchik, A. V., Petitjean, P., Balashev, S. A., et al. 2010, MNRAS, 404, 1583
- Leroy, A. K., Bolatto, A. D., Ostriker, E. C., et al. 2015, ApJ, 801, 25
- Leroy, A. K., Bolatto, A. D., Ostriker, E. C., et al. 2018, ApJ, 869, 126
- Levy, R. C., Bolatto, A. D., Leroy, A. K., et al. 2022, ApJ, 935, 19
- Lubowich, D. A., Pasachoff, J. M., Balonek, T. J., et al. 2000, Nature, 405, 1025
- Mangum, J. G., Ginsburg, A. G., Henkel, C., et al. 2019, ApJ, 871, 170
- Martín, S., Mangum, J. G., Harada, N., et al. 2021, A&A, 656, A46
- Martín, S., Martín-Pintado, J., Blanco-Sánchez, C., et al. 2019, A&A, 631, A159
- Martín, S., Mauersberger, R., Martín-Pintado, J., Henkel, C., & García-Burillo, S. 2006, ApJS, 164, 450
- Mauersberger, R., Henkel, C., & Chin, Y. N. 1995, A&A, 294, 23
- Müller, H. S. P., Schlöder, F., Stutzki, J., & Winnewisser, G. 2005, Journal of Molecular Structure, 742, 215
- Müller, H. S. P., Thorwirth, S., Roth, D. A., & Winnewisser, G. 2001, A&A, 370, L49
- Oliveira, C. M., Hébrard, G., Howk, J. C., et al. 2003, ApJ, 587, 235
- Prodanović, T. & Fields, B. D. 2003, ApJ, 597, 48
- Remijan, A., Biggs, A., Cortes, P. A., et al. 2019, ALMA Technical Handbook, ALMA Doc. 7.3, ver. 1.1, 2019, ALMA Technical Handbook, ALMA Doc. 7.3, ver. 1.1 ISBN 978-3-923524-66-2
- Roueff, E., Gerin, M., Lis, D. C., et al. 2013, Journal of Physical Chemistry A, 117, 9959
- Roueff, E., Parise, B., & Herbst, E. 2007, A&A, 464, 245
- Sánchez-Monge, A., Schilke, P., Schmiedeke, A., et al. 2017, arXiv:1704.01805 [astro-ph], arXiv: 1704.01805
- Tang, X. D., Henkel, C., Menten, K. M., et al. 2019, A&A, 629, A6
- Turner, B. E. 2001, ApJS, 136, 579
- Wooten, A. 1987, in Astrochemistry, ed. M. S. Vardya & S. P. Tarafdar, Vol. 120, 311–319
- Zahorecz, S., Jimenez-Serra, I., Testi, L., et al. 2017, A&A, 602, L3
- Zavarygin, E. O., Webb, J. K., Dumont, V., & Riemer-Sørensen, S. 2018, MNRAS, 477, 5536

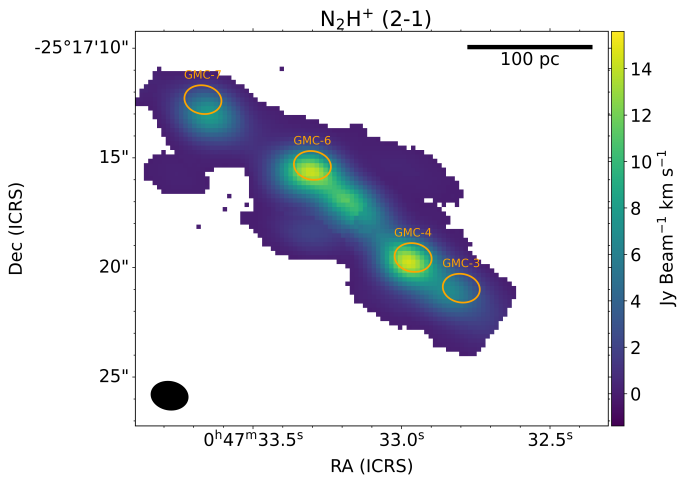


## Appendix A: Additional Spectral Information

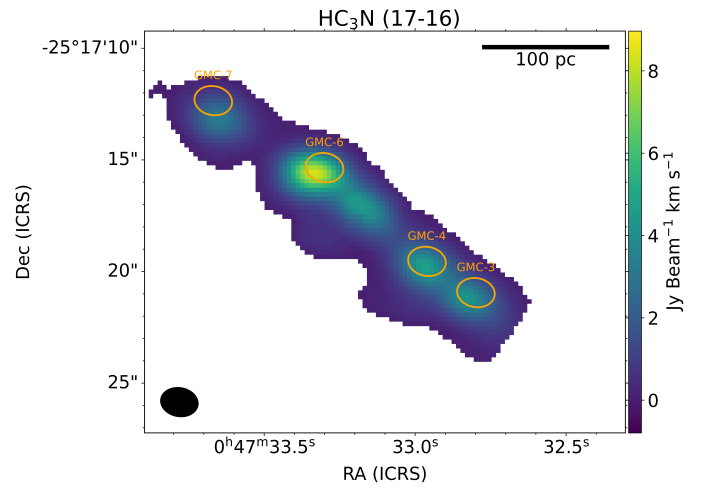
## Appendix B: Additional Moment 0 Maps

Table A.1: Spectroscopy of the HC<sub>3</sub>N and its isotopologues studied in this work from CDMS (Müller et al. 2001, 2005; Endres et al. 2016).

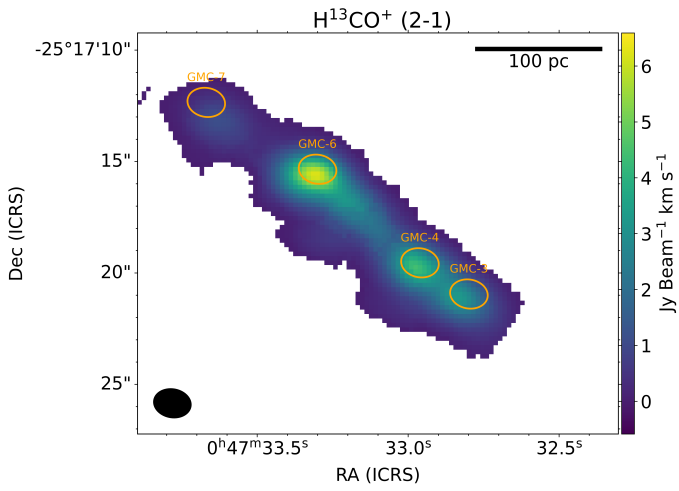
Molecule	Frequency (GHz)	Transition	logA <sub>ul</sub> (s <sup>-1</sup> )	E <sub>up</sub> (K)
HC <sub>3</sub> N	154.657284	17–16	-3.53575	66.8
HC <sub>3</sub> N	172.8493	19–18	-3.3896	83.0
HCC <sup>13</sup> CN	144.957454	16–15	-3.62088	59.1
HCC <sup>13</sup> CN	154.016078	17–16	-3.54113	66.5
HC <sup>13</sup> CCN	144.943467	16–15	-3.62109	59.1
HC <sup>13</sup> CCN	154.001217	17–16	-3.54134	66.5



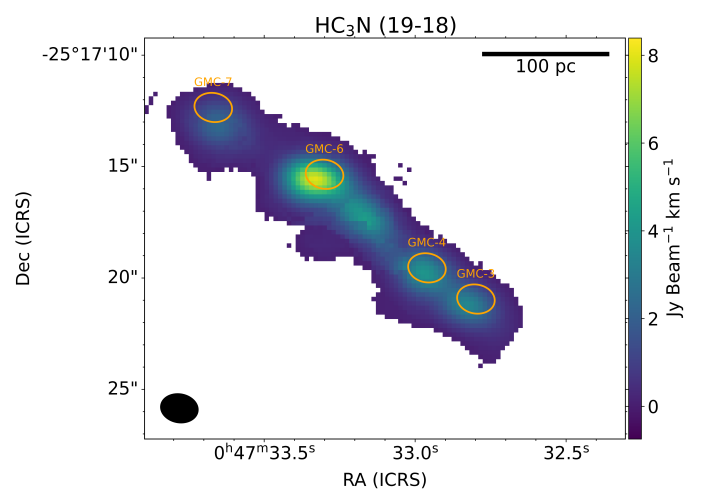
(a)



(a)



(b)



(b)

Fig. B.1: Velocity-integrated line intensity moment 0 maps, given in [ $\text{Jy km s}^{-1}/\text{beam}$ ], of the  $\text{N}_2\text{H}^+(2-1)$  and  $\text{H}^{13}\text{CO}^+(2-1)$  lines observed in the CMZ of NGC 253.

Fig. B.2: Velocity-integrated line intensity moment 0 maps, given in [ $\text{Jy km s}^{-1}/\text{beam}$ ], of the  $\text{HC}_3\text{N}(17-16)$  and  $\text{HC}_3\text{N}(19-18)$  lines observed in the CMZ of NGC 253.

## Appendix C: Spectra



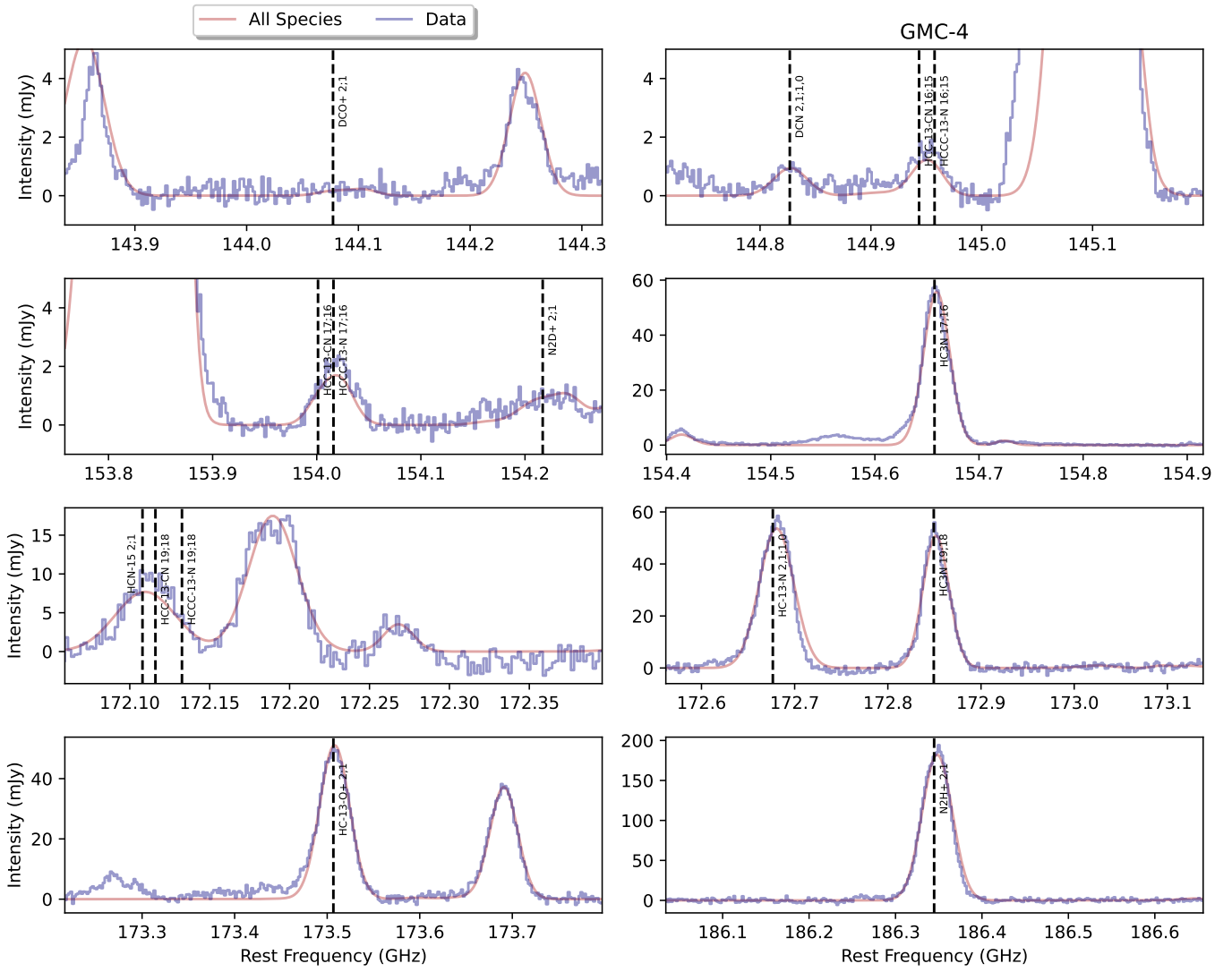


Fig. C.2: The spectra of selected lines observed in the region GMC-4 (in blue). The best fitting LTE model from MADCUBA is shown overlotted in red.

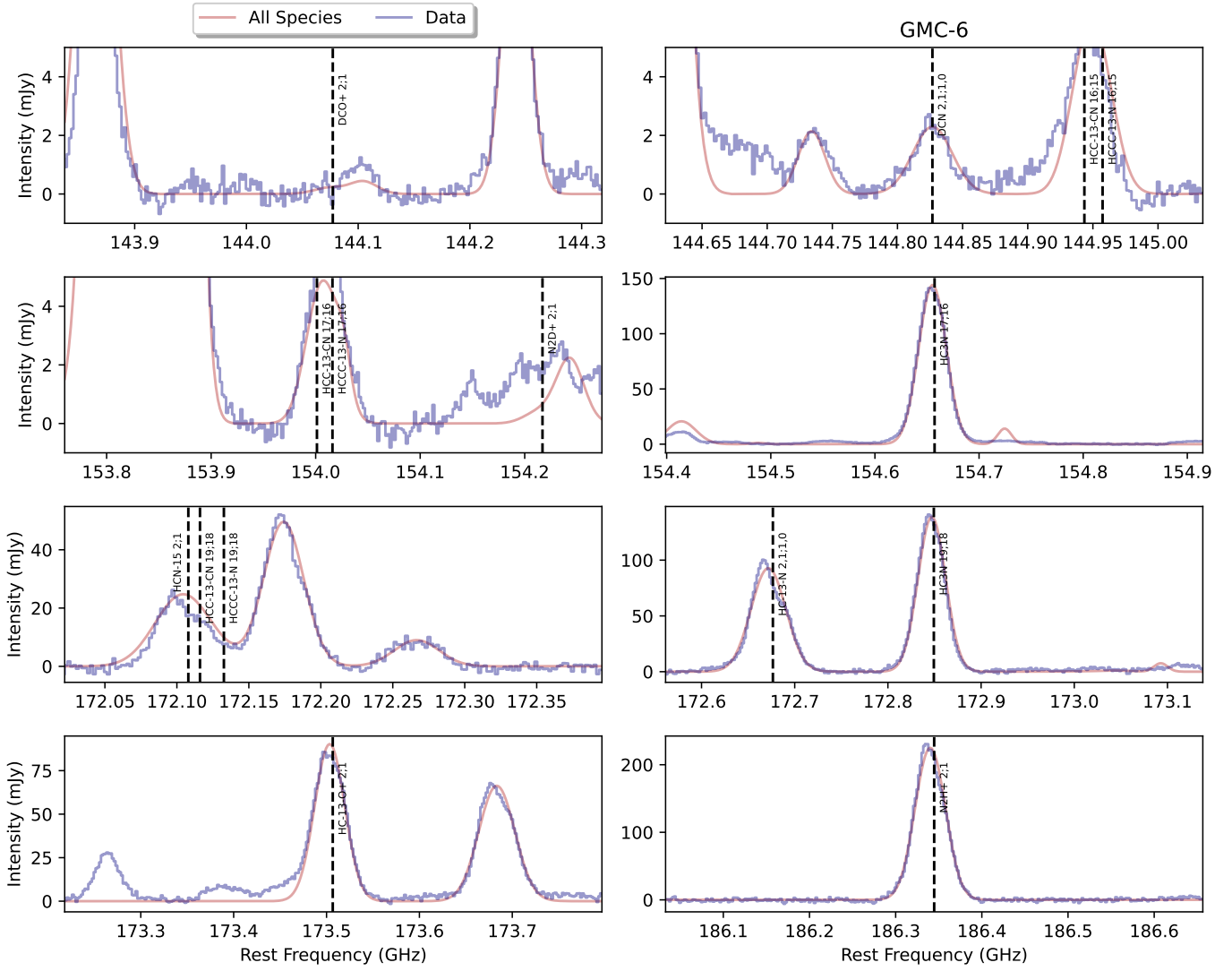


Fig. C.3: The spectra of selected lines observed in the region GMC-6 (in blue). The best fitting LTE model from MADCUBA is shown overplotted in red.

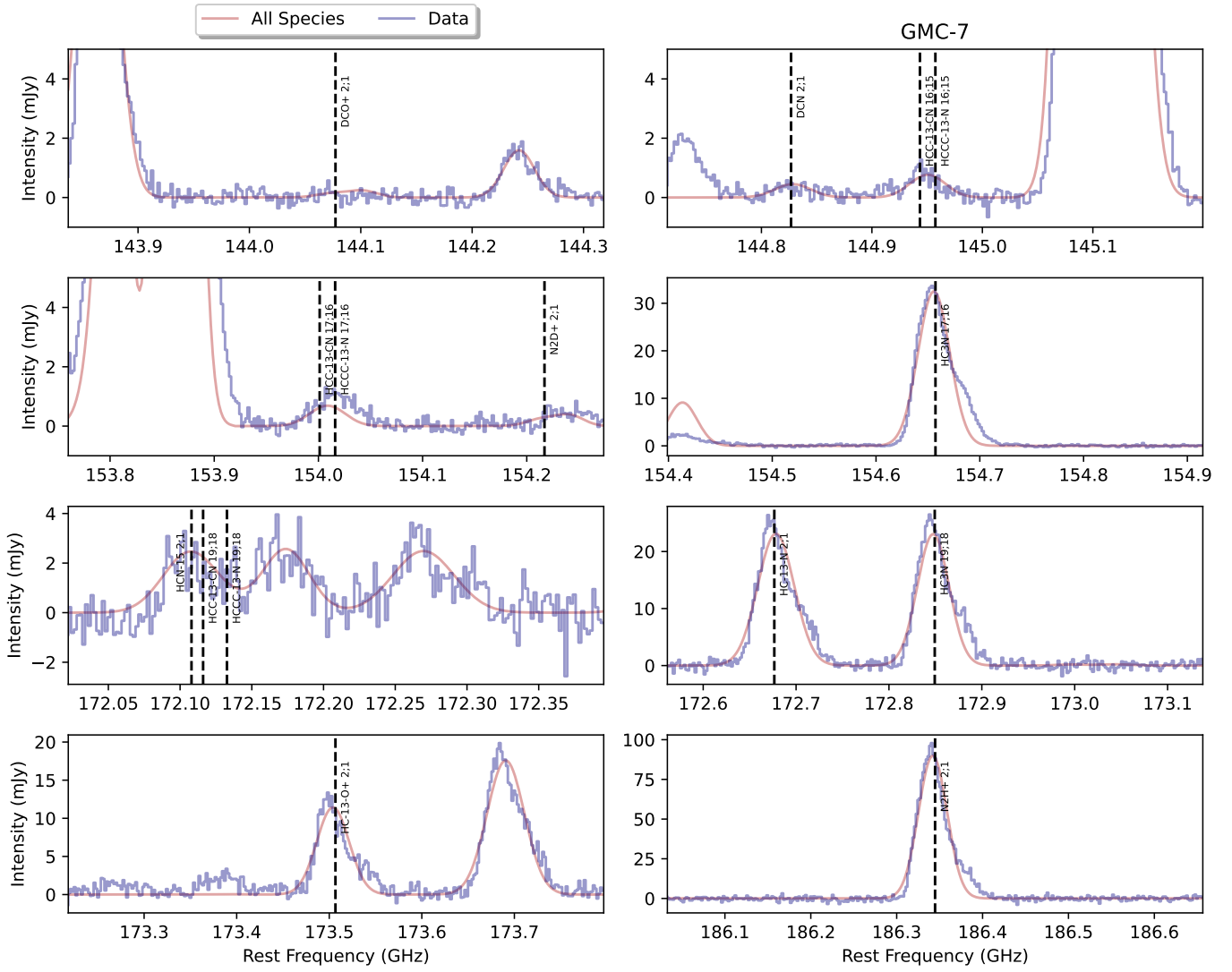


Fig. C.4: The spectra of selected lines observed in the region GMC-7 (in blue). The best fitting LTE model from MADCUBA is shown overlotted in red.